Final Draft
of the original manuscript:

Martins, R.M.S.; Schell, N.; Reuther, H.; Pereira, L.; Mahesh, K.K.;
Silva, R.J.C.; Braz Fernandes, F.M.:

Texture development, microstructure and phase transformation characteristics of sputtered Ni–Ti Shape Memory Alloy films grown on TiN<111>

In: Thin Solid Films (2010) Elsevier

DOI: 10.1016/j.tsf.2010.07.078

Texture development, microstructure and phase transformation characteristics of sputtered Ni-Ti Shape Memory Alloy films grown on TiN<111>

R.M.S. Martins [a,b,c,*], N. Schell [d], H. Reuther [b], L. Pereira [e], K.K. Mahesh [e], R.J.C. Silva [e], and F.M. Braz Fernandes [e]

[a] Unidade de Física e Aceleradores, Instituto Tecnológico e Nuclear, EN10, 2696-953 Sacavém, Portugal

[b] Institute of Ion Beam Physics and Materials Research, Forschungszentrum Dresden-Rossendorf, P.O. Box 510119, 01314 Dresden, Germany

[c] Centro de Física Nuclear da Universidade de Lisboa (CFNUL), Av. Prof. Gama Pinto 2, 1649-003 Lisboa, Portugal

[d] GKSS Research Center Geesthacht, Max-Planck-Str. 1, 21502 Geesthacht, Germany

[e] CENIMAT/I3N, Departamento de Ciência dos Materiais, Faculdade de Ciências e Tecnologia, FCT, Universidade Nova de Lisboa, 2829-516 Caparica, Portugal

Keywords: Shape Memory Alloy; Ni-Ti; sputtering; X-ray diffraction; texture; phase transformation

Abstract

Near equiatomic Ni-Ti films have been deposited by magnetron co-sputtering on TiN films with a topmost layer formed by <111> oriented grains (TiN/SiO_2/Si(100) substrate) in a chamber installed at a synchrotron radiation beamline. *In-situ* X-ray diffraction during Ni-Ti film growth and their complementary *ex-situ* characterization by Auger electron spectroscopy, scanning electron microscopy and electrical resistivity measurements during temperature cycling have allowed us to establish a relationship between the structure and processing parameters.

A preferential development of <110> oriented grains of the B2 phase since the beginning of the deposition has been observed (without and with the application of a substrate bias voltage of –45 and –90V). The biaxial stress state is considerably influenced by the energy of the bombarding ions, which is dependent on the substrate bias voltage value applied during the growth of the Ni-Ti film. Furthermore, the present work reveals that the control of the energy of the bombarding ions is a promising tool to vary the transformation characteristics of Ni-Ti films, as shown by electrical resistivity measurements during temperature cycling.

The *in-situ* study of the structural evolution of the growing Ni-Ti film as a consequence of changing the Ti:Ni ratio during deposition (on a TiN<111> layer) has also been performed. The preferential growth of <110> oriented grains of the Ni-Ti B2 phase has been as well observed despite the precipitation of Ti_2Ni during the deposition of a Ti-rich Ni-Ti film fraction. Functionally graded Ni-Ti films should lead to an intrinsic “two-way” shape memory effect which is a plus for the miniaturization of Ni-Ti films based devices in the field of micro-electro-mechanical systems.

1. Introduction

Ni-Ti Shape Memory Alloys (SMAs) are smart materials undergoing first order martensitic transformations driven by temperature and/or stress. The capability to transmit particularly high forces along with a large stroke makes Ni-Ti SMAs a material with the greatest specific work output of several actuation mechanisms. For comparison, bulk piezoelectric materials produce a large force over extremely small displacements, while piezo-bimorphs have large displacements but produce small forces [1,2]. Furthermore, when compared with the Ni-Ti bulk material, Ni-Ti films demonstrate fast cooling rates because of their higher surface/volume ratio, increasing substantially the heat transfer rate.

Ni-Ti SMAs films have been recognized as promising high performance materials in the field of micro-electro-mechanical systems (MEMS) [3-5]. Most applications of Ni-Ti films are focused on micro-actuators, such as micro-pumps, micro-grippers, micro-valves, micro-positioners, *etc.* [6]. Because of their sensitivity to environmental changes, e.g. thermal, and/or to stress they are also ideal materials for applications in micro-sensors [7].

Crystallized binary Ni-Ti SMAs transform martensitically from cubic B2 (CsCl type) austenite phase into monoclinic B19' phase either directly or via rhombohedral R–phase [1,8-10]. The martensitic transformation is a displacive type solid-state transformation and atoms are cooperatively rearranged or shifted into a new structure (without diffusion). The displacement of each atom is not large, but since the atoms move in the same direction in a domain or variant, the transformation results in a macroscopic change in shape. This phenomenon may lead to unique properties such

as the shape memory effect and superelasticity [11]. The R-phase can appear upon cooling and heating prior to martensite and austenite transformation, respectively. It is recognized as a martensitic transformation (martensite plates are observed by electron microscopy) and it exhibits an extremely small temperature hysteresis, which could be beneficial for many MEMS applications (e.g. actuators) [12].

One of the most important characteristics of SMAs is the temperature at which it changes from one crystalline structure to the other. The transformation temperatures are greatly dependent on composition, alloying elements and heat treatment processes [1]. In several cases, one percent change in composition can change the transformation temperatures by more than 100°C. In the Ni-Ti system, the Ni-rich side has some solubility at high temperature and the transformation temperatures are strongly dependent on the Ni concentration. Increasing Ni causes a drastic decrease in the transformation temperatures. The martensitic transformation temperature drops to below -173°C for a Ni content exceeding 51.5 at.% [13].

Nowadays, despite several methods proposed for resolving some of the processing difficulties, the deposition of Ni-Ti films with definite stoichiometry and high purity remains a challenge. Moreover, it is clear from the published works that important issues like the formation of film texture and its control are still unresolved. The study of the crystallographic texture of the Ni-Ti films assumes a major importance, since it has a strong influence on the extent of the strain recovery [14].

Considering potential applications in the field of MEMS, sputter deposition is a technique suited since the Ni-Ti films can be deposited directly on semiconductors or integrated circuits, and patterning can be as well incorporated using photoresist

technique. Typically, there is a need for an electrically and thermally insulating or sacrificial layer. Thus, our group has performed studies concerning the crystallization behaviour of Ni-Ti films deposited on different types of substrates (naturally oxidized Si(100) wafers, poly-Si and Si_3N_4 layers). The Ni-Ti films have been grown without intentional heating of the substrate [15,16]. Ni-Ti films have also been deposited on heated substrates (naturally and thermally oxidized Si(100) wafers, MgO single crystals and TiN layers). The deposition conditions to obtain the material fully crystallized at the end of the deposition have been optimised. Furthermore, the first experiments reported in the published literature concerning *in-situ* x-ray diffraction (XRD) investigations during Ni-Ti film growth have been presented [17]. It has been observed that an amorphous SiO_2 buffer layer induces the development of the (100) orientation of the B2 phase during deposition on heated substrates ($\approx$ 470ºC) [18,19]. A TiN buffer layer allows us a control of the crystallographic orientations of Ni-Ti films and acts as an efficient diffusion barrier. Ni-Ti films mainly containing grains with (110) or (211) planes of the B2 phase parallel to the film surface could be produced using TiN buffer layers [20,21]. These results improved the knowledge of Ni-Ti films texture formation and its control as well as substrate effects.

In a physical vapour deposition process like magnetron sputtering, it has been observed that along with other deposition parameters, the effect of the ion bombardment also plays an important role on the properties of the growing film [22-24]. Ion bombardment influences film properties such as packing density, surface roughness, and crystallinity. Energetic ion, electron, or neutral bombardment of the growing film surface can alter the mobility of film atoms, resulting in changes of the film structure or density. Therefore, it has been concluded that the control of the ion bombardment energy would be one of the key factors in determining the microstructure

and properties of the Ni-Ti films. The previous experiments performed by the group have shown a preferential growth of <110> oriented grains of the Ni-Ti B2 phase from the beginning of the deposition, with a constant growth rate during the whole deposition, for Ni-Ti films deposited on TiN with a topmost layer formed by <111> oriented grains (<hkl> grains are here defined as grains with a plane from the {hkl} family parallel to the film surface) [20,21]. These depositions were carried out without a bias voltage (V_b) applied to the substrate. Here, the effect of a negative V_b applied to the substrate [SiO_2/Si(100) with a TiN layer] during the Ni-Ti growth on the microstructure and transformation characteristics of the films is revealed.

Future directions include the production of functionally graded films by changing deliberately the Ti:Ni ratio across their thickness (i.e., different phase transformation temperatures). The main goal is the fabrication of films with a “two-way” reversible actuation (films with a combination of superelasticity and shape memory characteristics) [6,25]. However, the growth process is a highly complex phenomenon controlled by many parameters requiring the application of several experimental tools to understand the physical processes occurring during deposition.

In the present study, a Ni-Ti film with approximately half of its thickness with a near equiatomic composition and the other half Ti-rich has been deposited. Typically a film with such compositional discrepancy exhibits different transformation temperatures for the different film fractions. When heating it a little above room temperature (RT) the Ti-rich fraction is expected to exhibit still the martensitic structure. Due to the different mechanical properties of martensite and austenite phases a curvature should thus be observed (due to a constraint) serving as a functionally graded bimorph. It is important to know the trend of the B2 phase preferred orientation for an increase of the Ti content.

This is a typical question that could be answered taking profit of the unique equipment used in the present work.

2. Experimental details

Ni-Ti films have been grown and the in-situ XRD studies have been carried out at the Rossendorf Beamline at the European Synchrotron Radiation Facility. The Materials Research Hutch (MRH) combines the reliable and stable bending magnet X-ray source characteristics with high flux, low divergence, and energy tunability in a broad range of hard X-rays with an ample and precise sample positioning, enhanced by special sample environments [26]. A sputtering deposition chamber has been inserted into the six-circle diffractometer of the MRH [27]. It is equipped with two-unbalanced miniature magnetrons each positioned at a distance of 100 mm from the substrate and tilted 30° away from the substrate normal. Ni-Ti (49 at% Ni – 51 at% Ti) and 99.99% pure Ti disks of 25.4 mm diameter were used as targets.

Polycrystalline films have been grown onto thermally oxidized Si(100) substrates (15×15 mm^2, with a 140 nm amorphous SiO_2 capping layer). To obtain TiN films (thickness of ≈ 215 nm, i.e., 41 min deposition time) with a topmost layer constituted by <111> oriented grains, a substrate temperature of 470°C has been selected and the working pressure (flux ratio $Ar/N_2 = 4/1$) was set to 0.35 Pa. A V_b of –30 V has been applied to the substrate during the TiN film growth while the Ti target was running at a constant power of 80 W.

For the deposition of near equiatomic Ni-Ti films, the Ni-Ti and Ti magnetrons were driven for ≈120 min at a power of 40 and 20 W, respectively (Ar working pressure was set to 0.42 Pa), resulting in final thickness values of approximately 760±50 nm.

The depositions of the Ni-Ti films have been performed with three different biasing conditions, viz., without V_b, with V_b of −45 V and with V_b of −90 V (Table 1).

The Ni-Ti and Ti magnetrons were driven during 60 min at a power of 40 and 20 W (film composition of ≈ 50 at%Ti), respectively and additionally for 69 min at a power of 40 and 25 W (≈ 55 at%Ti) for the deposition of the graded film. A V_b of -45 V was applied to the substrate during the Ni-Ti deposition (last row in Table 1).

The radiation was monochromatized to λ = 0.0675 nm (18.367 keV) and large angle XRD in Bragg–Brentano geometry has been employed, thus probing the diffraction vector situated in a plane perpendicular to the plane of deposition. A sequence of scans has been performed during Ni-Ti film processing in order to monitor the B2(110) and B2(200) XRD peaks; these scans are intended to reveal the type of preferential orientation and to determine off-plane lattice parameter variations.

Scanning Electron Microscopy (SEM) and atomic force microscopy (AFM) have been used to characterize the surface morphology of the Ni-Ti films at RT. The SEM observations have been carried out on a Hitachi S-4800 using an accelerating voltage of 10 kV, an emission current of 10.2 µA, a working distance of 7.2 mm and a magnification of x150 000. The AFM studies have been performed on an Asylum Research MFP3D-AFM (Santa Barbara, USA), AC Mode imaging, using AC240TS silicon cantilevers (Olympus, spring constant k≈2N/m).

The temperature dependence of the electrical resistivity (ER) of the samples has been measured using the four-probe van der Pauw geometry (BIO-RAD HL 5550) in order to investigate the phase transformations characteristics of the samples. The

thermal cycles comprised (i) heating from RT up to 110°C, followed by (ii) cooling down to –110°C, and finishing by (iii) heating up to 110°C. The analysis of the transformation characteristics has been based on the cycles (ii) and (iii). The measurements have been performed with the Ni-Ti films attached to the substrate.

Auger Electron Spectroscopy (AES) in conjunction with ion sputtering has been used to obtain depth profiles of elemental distribution in the films. The experiments have been carried out on a scanning Auger electron spectrometer Microlab 310F (Fisons) with field-emission cathode and hemispherical sector analyzer. An Ar ion beam with energy of 3 keV has been used for sputtering and an electron beam of about 1 µm diameter has been used for the sputter profiles (with sample rotation).

3. Results

3.1. Growth of near equiatomic Ni-Ti films (no V_b, -45 V and –90 V)

The effect of V_b on the growth of near equiatomic Ni-Ti films on a TiN buffer layer of thickness ≈ 215 nm (topmost layer formed by <111> oriented grains) has been investigated. The applied V_b values were –45 and –90 V. The evolution of the B2(110) and B2(200) diffraction peaks during the processing of the Ni-Ti films at 470°C have been followed *in situ* by XRD. There was a preferential growth of <110> oriented grains of the Ni-Ti B2 phase from the beginning of the deposition, with a constant rate up to the end of the deposition. Nevertheless, the increase in V_b to –90 V led to a decrease of the intensity of the B2(110) diffraction peak. The XRD patterns for this set of samples obtained after deposition at ≈ 470°C and at RT are presented in Fig. 1. The results obtained at high temperature (austenitic state) show a higher intensity and a lower value of the full width at half maximum (FWHM) for the Ni-Ti films deposited with

V_b (Fig. 1 (top)). A decrease of the FWHM value with increasing V_b is also seen in Fig. 1 (top). The results presented in Fig. 1 (bottom) show that the film deposited without V_b exhibits the presence of the R-phase at RT, which has not been detected for the other two samples.

The a_0 values of the B2 phase of the Ni-Ti films have been calculated from the position of the B2(110) diffraction peak recorded during Ni-Ti film growth and, thus, they could be represented as a function of deposition time. A continuous decrease of the a_0 value of the B2 phase during the deposition of the Ni-Ti film without V_b has been observed (Fig. 2). The deposition with –45 V led to a slight decrease of the a_o at the beginning of the deposition, followed by a stabilization. Increasing the V_b further to –90 V, showed a practically constant value of a_o during the whole deposition. It can be observed that as the V_b was increased, the a_o value decreased, approaching the equilibrium value of ≈ 0.303 nm for an applied bias of –90 V.

Figure 3 (a-c) shows SEM micrographs of the surface morphology of the Ni-Ti film, deposited without applying V_b, with V_b of –45 and –90 V, respectively. The microstructure of the films was influenced by the degree of ion bombardment (due to V_b). The increase in ion energy by applying a V_b of –45 V led to apparently larger crystals in the form of regular polyhedron visible on the surface of the film. A further increase of V_b to –90 V led to the appearance of surface steps on the crystals. This is also noticeable in the AFM micrograph presented in Fig. 3 (d).

The effect of the microstructural changes in the Ni-Ti films (due to applied V_b) on their transformation characteristics has been examined by ER measurements during thermal cycling. The ER results obtained for this set of samples are shown in Fig. 4. The pronounced increase in resistivity in the cooling and heating cycles has been

attributed to lattice distortion and twinning, which are dominant mechanisms in self-accommodation R-phase transformation (both forward and reverse). The Ni-Ti film deposited without applying V_b exhibited higher R-phase transformation temperatures. Furthermore, the increase of the resistivity during R-phase distortion on cooling for the Ni-Ti sample deposited with a V_b of −90 V was not as high as for the other two samples.

The transformation temperatures also depend on composition. In order to detect a possible compositional effect on the transformation characteristics of this set of samples, AES was used to obtain depth profiles of elemental distribution in the films. In Fig. 5 results are presented concerning the Ni-Ti films deposited without V_b and with applying a V_b of −90 V. The Ni-Ti film deposited without V_b exhibits a slightly higher Ni content. Increasing the Ni-content causes a decrease in the transformation temperatures but this is not the case.

3.2. Controlled change of the Ti:Ni ratio during film growth (V_b of −45 V)

Figure 6 (top) shows the variation of the net areas of the B2(110) diffraction peak, obtained from the *in-situ* XRD data, for the growth of the near equiatomic and graded Ni-Ti films on top of the TiN buffer layer *versus* time (films deposited with a V_b of −45 V). The variation of the net areas of the Ti_2Ni(333/511) diffraction peak for the graded Ni-Ti film is also presented. A preferential development of <110> oriented grains of the Ni-Ti B2 phase from the beginning of the deposition, with a constant growth rate during the whole deposition was observed. The precipitation of the Ti_2Ni phase was detected in the second step of the deposition of the graded film (Ti power = 25 W) by the presence of the Ti_2Ni(333/511) diffraction peak (with low intensity). A slight increase of the a_0 values of the B2 phase as calculated from the

B2(110) diffraction peak position was observed during this second deposition period, which has not been observed for the deposition of the near equiatomic Ni-Ti film (evolution of a_0 values of the samples are represented in Fig. 6 (bottom)). In the case of the a_0 values of the Ti_2Ni a continuous gradual decrease was perceptible as the film is grown.

The temperature dependence results of the ER of the Ni-Ti graded film are shown in Fig. 7 for cooling and heating (together with the results obtained for the near equiatomic film). On cooling, there was a resistivity increase associated with the B2 $\Rightarrow$ R-phase transformation, followed by a resistivity decrease due to the R-phase $\Rightarrow$ B19' transformation. During heating, a similar increase of the ER was not detected. However, an increase of the ER could be observed for the near equiatomic film during heating (R-phase$\Rightarrow$ B2 transformation). In contrast, the resistivity results recorded for the Ni-Ti graded film have shown that a big fraction of the film was already transformed to B19' at RT, while the near equiatomic Ni-Ti film exhibits lower transformation temperatures.

4. Discussion

The *in-situ* XRD results obtained during the deposition of the Ni-Ti films without V_b on TiN<111> have shown a preferential development of <110> oriented grains of the B2 phase from the beginning of the deposition. It is generally assumed that for most bcc metals the lowest surface energies correspond to the (110) plane, as predicted from calculations [28]. Due to surface energy minimization, (110) texture is favored in bcc films. This is apparently valid for the preferential growth of <110> oriented grains of the Ni-Ti B2 phase.

Analogously, the experiments have also shown that the B2(200) diffraction peak did not assume an important relevance. It has been shown in Ref [18] that an amorphous SiO_2 buffer layer induces the development of the (100) orientation of the B2 phase during deposition on heated substrates. As it is revealed in the present work, for depositions on TiN buffer layers there is no Ni-Ti/SiO_2 interface and, thus, the development of the (100) orientation parallel to the substrate surface is not observed. Instead, a preferential development of (110) planes of the Ni-Ti B2 phase parallel to the substrate surface is observed since the beginning of Ni-Ti film deposition.

Similarly, the preferential growth of <110> oriented grains of the B2 phase from the beginning of the deposition with a constant growth rate during the whole deposition has also been observed with applied V_b (–45 and –90 V). However, a decrease of the FWHM values of the Bragg peaks for the Ni-Ti films deposited with V_b has been observed [Fig. 1(top)]. This suggests an overall trend of increasing coherence domain length with increasing V_b. SEM observations, performed *ex-situ*, have shown that the microstructure of the Ni-Ti films was influenced by the degree of ion bombardment (Fig. 3). The SEM micrographs indicate that the increase in ion energy by using V_b (–45 and –90 V) led to apparently larger crystals in the form of regular polyhedron (visible on the film surface). This observation is consistent with the trend observed *in situ* by XRD, i.e., a decrease in the FWHM value with increasing V_b.

The decrease of the a_o value of the B2 phase for the Ni-Ti film deposited without V_b as a function of deposition time (Fig. 2) suggests that the film experiences a biaxial compressive stress state, which is relaxed with increasing film thickness (approaching ≈ 0.304 nm at the end of the annealing step). The analysis of the variation of the a_0 values for the Ni-Ti B2 phase of the film deposited with a V_b of –45 V has shown a very small decrease of a_0 at the beginning of the deposition, followed by a

stabilization near the value of 0.303 nm. A further increase to −90 V showed a practically constant value of a_0 during the whole deposition process. It is then possible to conclude that as V_b is increased (within the range used in this work), the a_0 value of B2 phase decreases, approaching the equilibrium value of ≈ 0.303 nm for −90 V applied. This variation of the a_0 values suggests a relaxation of the biaxial compressive stress state resulting from the higher energetic ion bombarding. This indicates that an increase of energy of the incident ions resulted in enhanced mobility of the adatoms allowing them to diffuse on the substrate surface and, as a result, the adatoms are less kinetically constrained.

The study of this set of Ni-Ti samples deposited without V_b, with −45 and −90 V on a TiN<111> buffer layer (Fig. 4) has revealed higher R-phase transformation temperatures for the sample deposited without V_b. An effect of compositional difference is not expected as confirmed by the AES results presented in Fig. 5. The composition of both films is near equiatomic with only a slight Ni enrichment for the film deposited without V_b. In the case of the deposition with V_b of –90 V the Ni content is lower since there is a Ni re-sputtering due to its higher sputter yield (when compared with the one of Ti). For a possible role of the composition on the increase of transformation temperatures, a higher Ti content would be expected for the film deposited without V_b. It should also be mentioned that the XRD data recorded for these near equiatomic films did not show the presence of precipitates. At the moment, it is possible to conclude that the Ni-Ti film deposited without V_b exhibits higher a_o values for the B2 phase, i.e. the sample exhibiting higher R-phase transformation temperatures. It is suggested that a biaxial stress state could play a role on the transformation characteristics of the different samples. The data collected during the present experiments will be complemented with further studies.

The lower increase of the resistivity during R-phase distortion (on cooling) for the Ni-Ti film grown with V_b of −90 V is the result of the higher energetic ion bombardment. An increase of V_b from −45 to −90 V led to the appearance of surface steps on the crystals (Fig. 3). The ER results are consistent with the assumption that spatial constraints introduced by the higher energetic bombardment (−90 V) in the microstructure of the film could generate a resistance force for lattice distortion and twinning. The increase in negative V_b leads, in general, to a higher energy of the incident ions leading to an increase in the grain size because of the increase in adatom mobility, as shown above. Nevertheless, it should be taken in consideration that a sufficiently high voltage can lead to increased defect formation. As the ion energy is increased, the film volume affected by the ions becomes larger giving rise to defect generation at increasingly larger distances below the growth surface, thus reducing the probability of the point defects becoming annihilated.

The effect of the controlled change of the Ti:Ni ratio during the deposition of a Ni-Ti film (with a V_b of −45 V) on a TiN buffer layer has been tested (Ni-Ti film half thickness near equiatomic composition and half thickness Ti-rich). The precipitation of the Ti_2Ni phase in the second step of the deposition (due to the increase of the power of the Ti target) did not affect the preferential growth of <110> oriented grains of the Ni-Ti B2 phase (Fig. 6). At the initial deposition stage (Ti power = 20 W), considering the evolution of the a_0 values of the B2 phase, a slight stress relaxation takes place suggesting that the film experiences a biaxial compressive stress state, which is relaxed with increasing thickness. With the increase of Ti content (Ti power = 25 W), and, thus Ti_2Ni precipitation, a_0 values start rising again. During the precipitation

process the a_0 value of Ti_2Ni slightly decreases in a gradual way. This could be associated with the formation of a stress field around the precipitate [29].

The ER *versus* temperature response of the Ni-Ti graded film during thermal cycling shows higher transformation temperatures when compared with the near equiatomic Ni-Ti film (Fig. 7). While heating around RT, the films structure is mainly martensitic and while cooling R-phase transformation starts around 70°C. It is believed that in this case this is due to the higher Ti content in the Ni-Ti graded film together with the presence of a biaxial stress state.

The experimental procedure adopted led to a good understanding of the relationship among processing, microstructure and properties of near equiatomic and graded Ni-Ti SMAs films on TiN<111>, which is a plus for their successful implementation in MEMS.

5. Conclusions

The characterization of sputtered near equiatomic Ni-Ti films, on TiN with the topmost layers formed by <111> oriented grains, has been presented. A preferential development of grains with (110) planes of the B2 phase parallel to the film surface has been observed since the beginning of the deposition. There is an overall trend of increasing coherence domain length with increasing V_b and the biaxial compressive stress state in the Ni-Ti films is reduced when V_b is applied during the deposition process, which has been associated with the higher adatoms mobility. These differences lead to distinct transformation characteristics, as observed by electrical resistivity measurements during thermal cycling of the Ni-Ti films.

The deposition of Ni-Ti graded films has been performed leading to an improvement of the knowledge of their structural development (phase formation/strain evolution). Enrichment of Ti in the film matrix and the biaxial stress state led to higher phase transformation temperatures. The knowledge acquired during these experiments is useful for the optimization of the deposition parameters in order to fabricate films with a “two-way” actuation. It will lead to the development of smaller devices due to an optimal design of microdevices regarding size and weight (i.e., no consideration has to be paid to a resetting spring).

Acknowledgements

The authors would like to thank the FCT/MCTES for a Ph.D. and a Post-Doctoral grant (POCI 2010/FSE for R.M.S.M.), E. Fortunato for the use of the four-probe-apparatus for the electrical resistivity measurements at CENIMAT/I3N and U. Strauch for his technical assistance during the measurements at ROBL. The Asylum Research Company is also kindly acknowledged for facilitating the AFM experiments, which have been performed by A. Moshar. Financial support from the FCT/MCTES for the pluriannual financial support of CFNUL and CENIMAT/I3N is gratefully acknowledged by R.M.S.M and L.P., K.K.M., R.J.C.S., F.M.B.F, respectively. Financial support from the ESRF for the experiments at ROBL is as well acknowledged by K.K.M., R.J.C.S. and F.M.B.F.

References

_[1] K. Otsuka, X. Ren, Prog. Mater. Sci. 50 (2005) 511.

_[2] A. Ishida, V. Martynov, MRS Bull. 27 (2002) 111.

_[3] R.H. Wolf, A.H. Heuer, J. Microelectromech. Syst. 4 (1995) 206.

_[4] P. Krulevitch, A.P. Lee, P.B. Ramsey, Trevino J.C., Hamilton J., Northrup M.A., J. Microelectromech. Syst. 5 (1996) 270.

_[5] H. Kahn, M.A. Huff, A.H. Heuer, J. Micromech. Microeng. 8 (1998) 21.

_[6] Y. Fu, H. Du, W. Huang, S. Zhang, M. Hu, Sens. Actuators A 112 (2004) 395.

_[7] M. Bendahan, K. Aguir, J.L. Seguin, H. Carchano, Sens. Actuators 74 (1999) 242.

_[8] D. Shindo, Y. Murakami, T. Ohba, MRS Bull. 27 (2002) 121.

_[9] H. Sitepu, W.W. Schmahl, D.M. Toebbens, Textures Microstruct. 35 (2003) 185.

_[10] T. Goryczka, H. Morawiec, J. Alloys Compd. 367 (2004) 137.

_[11] K. Otsuka, T. Kakeshita, MRS Bull. 27 (2002) 91.

_[12] P. Šittner, M. Landa, P. Lukáš, V. Novák, Mech. Mater. 38 (2006) 475.

_[13] W. Tang, Metall. Mater. Trans. 28A (1997) 537.

_[14] Y.C. Shu, K. Bhattacharya, Acta Mater. 46 (1998) 5457.

_[15] R.M.S. Martins, F.M.B. Fernandes, R.J.C. Silva, L. Pereira, P.R. Gordo, M.J.P. Maneira, M. Beckers, A. Mücklich, N. Schell, Appl. Phys. A 83 (2006) 139.

_[16] R.M.S. Martins, N. Schell, P.R. Gordo, M.J.P. Maneira, R.J.C. Silva, F.M.B. Fernandes, Vacuum 83 (2009) 1299.

_[17] R.M.S. Martins, N. Schell, R.J.C. Silva, F.M.B. Fernandes, Nucl. Instrum. Methods Phys. Res., Sect. B 238 (2005) 319.

_[18] R.M.S. Martins, N. Schell, M. Beckers, K.K. Mahesh, R.J.C. Silva, F.M.B. Fernandes, Appl. Phys. A 84 (2006) 285.

_[19] R.M.S. Martins, N. Schell, M. Beckers, R.J.C. Silva, K.K. Mahesh, F.M. Braz Fernandes, Mater. Sci. Eng. A 481/482 (2008) 626.

_[20] R.M.S. Martins, N. Schell, R.J.C. Silva, L. Pereira, K.K. Mahesh, F.M.B. Fernandes, Sens. Actuators B 126 (2007) 332.

_[21] R.M.S. Martins, N. Schell, K.K. Mahesh, L. Pereira, R.J.C. Silva, F.M. Braz Fernandes, J. Mater. Eng. Perform. 18 (2009) 543.

_[22] J.A. Thornton, J. Vac. Sci. Technol. A 4 (1986) 3059.

_[23] C.A. Davis, Thin Solid Films 226 (1993) 30.

_[24] K.P. Almtoft, J. Bøttiger, J. Chevallier, N. Schell, R.M.S. Martins, J. Mater. Res. 20 (2005) 1071.

_[25] R.M.S. Martins, N. Schell, A. Mücklich, H. Reuther, M. Beckers, R.J.C. Silva, L. Pereira, F.M. Braz Fernandes, Appl.Phys. A 91 (2008) 291.

_[26] W. Matz, N. Schell, G. Bernhard, F. Prokert, T. Reich, J. Claußner, W. Oehme, R. Schlenk, S. Dienel, H. Funke, F. Eichhorn, M. Betzl, D. Pröhl, U. Strauch, G. Hüttig, H. Krug, W. Neumann, V. Brendler, P. Reichel, M.A. Denecke, H. Nitsche, J. Synchroton Radiat. 6 (1999) 1076.

_[27] N. Schell, J. Borany, J. Hauser, in: J.-Y. Choi, S. Rah (Eds.), 9th International Conference on Synchrotron Radiation Instrumentation, Daegu, South Korea, May 28-June 2, 2006, Synchrotron Radiation Instrumentation 879 (2007) 1813.

_[28] J.-M. Zhang, F. Ma, K.-W. Xu, Surf. Interf. Anal. 35 (2003) 662.

_[29] A. Ishida, K. Ogawa, M. Sato, S. Miyazaki, Metall. Mater. Trans. A 28 (1997) 1985.

Figure captions

Figure 1. XRD patterns obtained for the Ni-Ti films deposited without V_b, with −45 and −90 V on TiN<111> buffer layers; top - after deposition at ≈ 470°C, bottom - at RT.

Figure 2. The a_o values as obtained from the positions of the B2(110) diffraction peaks of the Ni-Ti films grown with different V_b applied represented as a function of processing time.

Figure 3. SEM micrographs showing the effect of the V_b on the surface morphology of Ni-Ti films: (a) deposited without V_b, (b) with −45 V and (c) with −90 V on TiN<111> buffer layers. An AFM micrograph of the Ni-Ti film deposited with −90 V is shown in (d).

Figure 4. Dependence of the ER with temperature for the Ni-Ti samples deposited without V_b, with −45 and −90 V on a TiN<111> buffer layer; during cooling (top) and during heating (bottom).

Figure 5. AES elemental concentration profiles for the Ni-Ti samples on TiN<111> buffer layers: top - Ni-Ti deposited without V_b, bottom - deposition using a V_b of −90 V.

Figure 6. In-situ XRD results for the Ni-Ti samples (near equiatomic and graded Ni-Ti films) deposited with −45 V on a TiN<111> buffer layer. Represented are the net areas of the Bragg-Brentano B2(110) and Ti_2Ni(333/511) diffraction peaks as well as the a_0 values as obtained from the positions of the respective diffraction peaks, as a function of deposition time.

Figure 7. Dependence of the ER with temperature for the Ni-Ti samples (near equiatomic and graded Ni-Ti films) deposited with −45 V on a TiN<111> buffer layer.

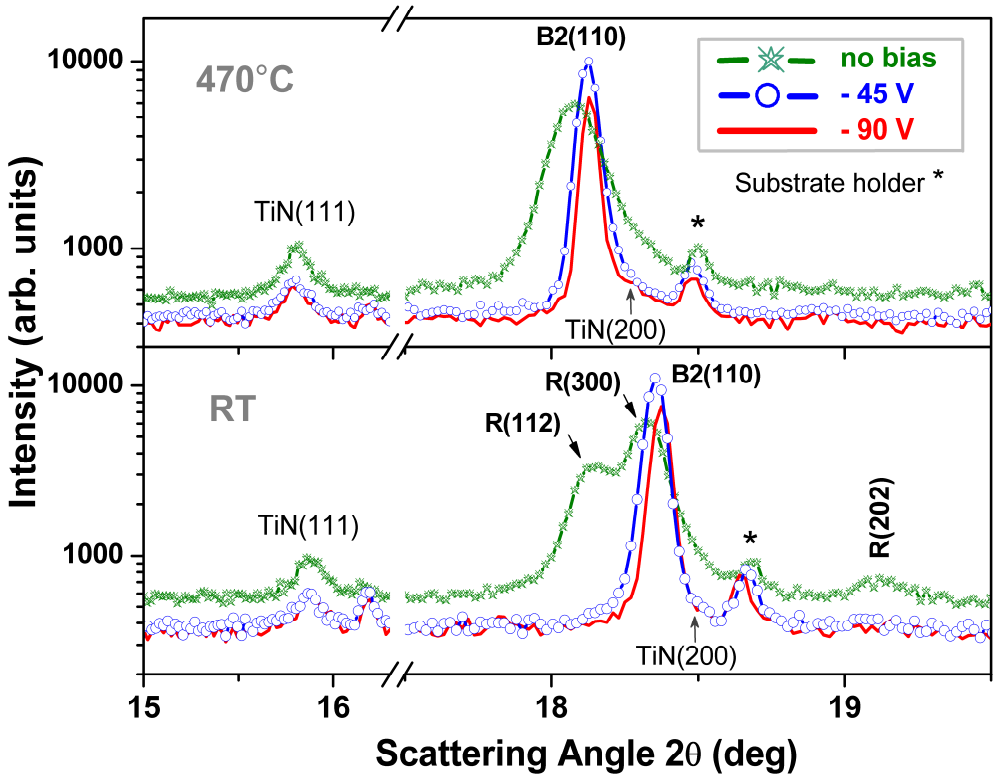
470°C
B2(110)
no bias
- 45 V
- 90 V
Substrate holder *
TiN(111)
*
TiN(200)
RT
R(300)
B2(110)
R(112)
TiN(111)
*
R(202)
TiN(200)
10000
1000
10000
1000
15
16
18
19
Intensity (arb. units)
Scattering Angle 2θ (deg)

FIGURE 1

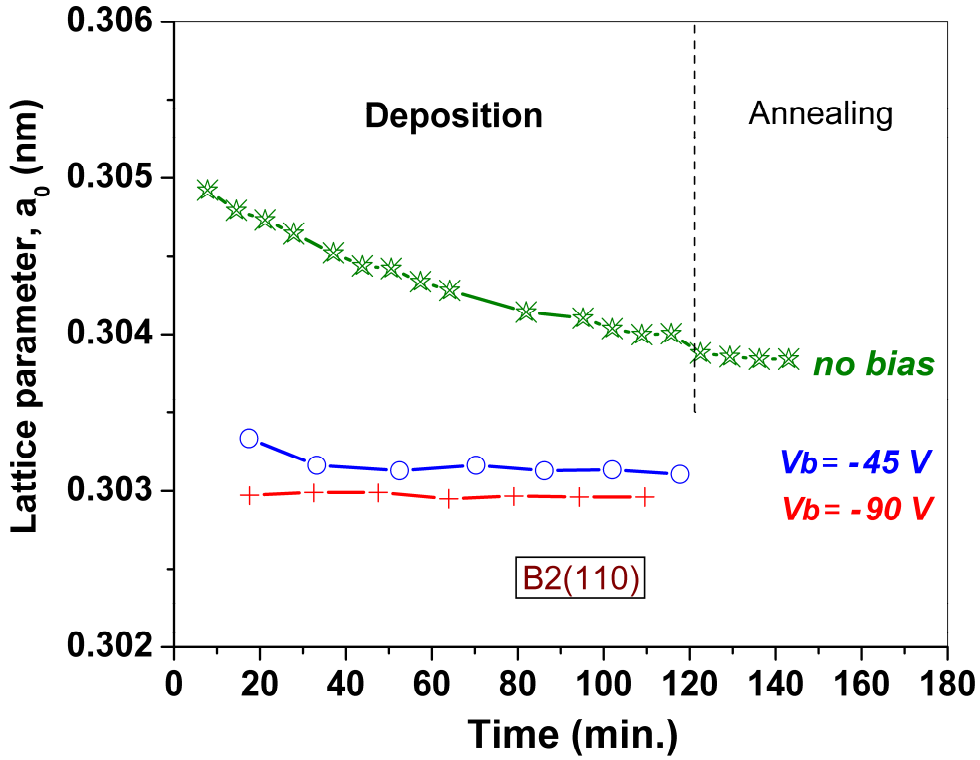
Deposition
Annealing
no bias
Vb = -45 V
Vb = -90 V
B2(110)
Lattice parameter, a0 (nm)
Time (min.)
0.306
0.305
0.304
0.303
0.302
0
20
40
60
80
100
120
140
160
180

FIGURE 2

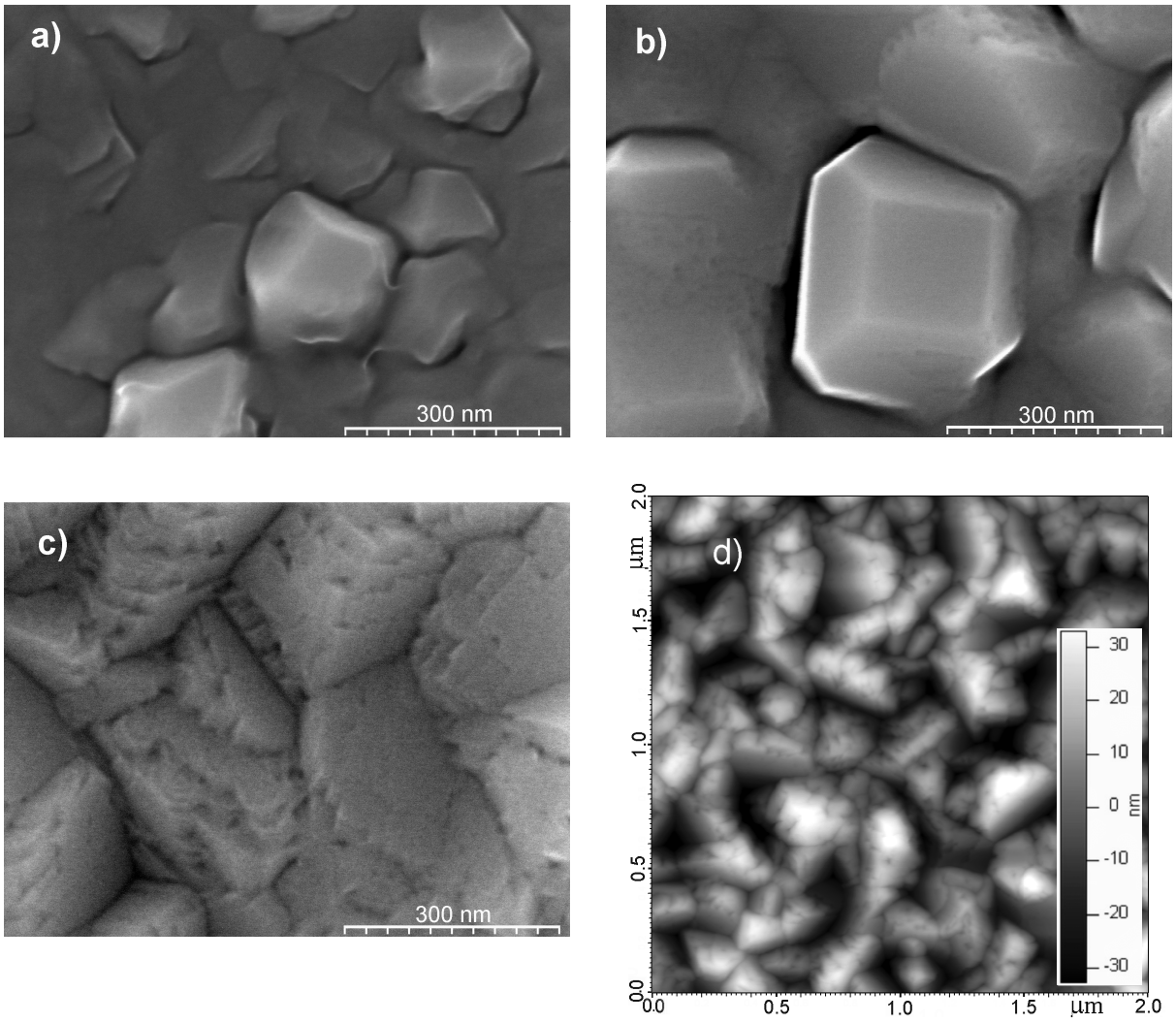
a)
300 nm
b)
300 nm
c)
300 nm
d)
µm
2.0
1.5
1.0
0.5
0.0
0.0
0.5
1.0
1.5
µm
2.0
30
20
10
0
-10
-20
-30
nm

FIGURE 3

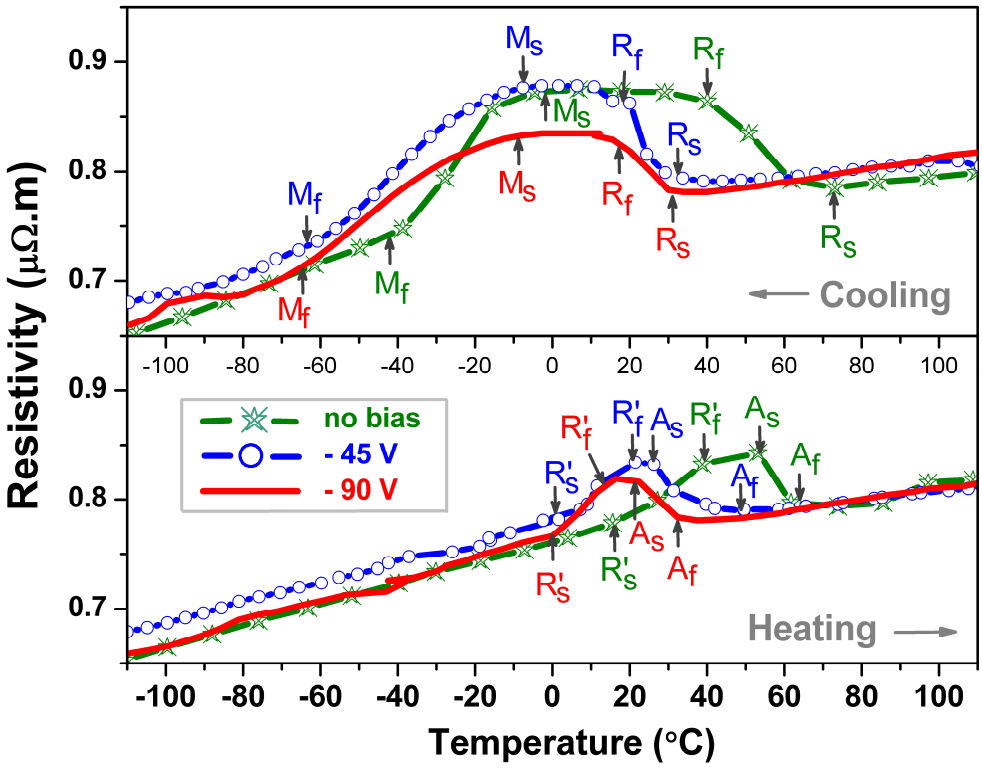
Resistivity (μΩ.m)
0.9
0.8
0.7
Ms
Rf
Rf
Ms
Rs
Mf
Ms
Rf
Rs
Rs
Mf
Mf
Cooling
-100
-80
-60
-40
-20
0
20
40
60
80
100
no bias
- 45 V
- 90 V
R'f
R'f
As
R'f
As
Af
R'f
Af
R's
As
R's
Af
R's
Heating
Temperature (°C)

FIGURE 4

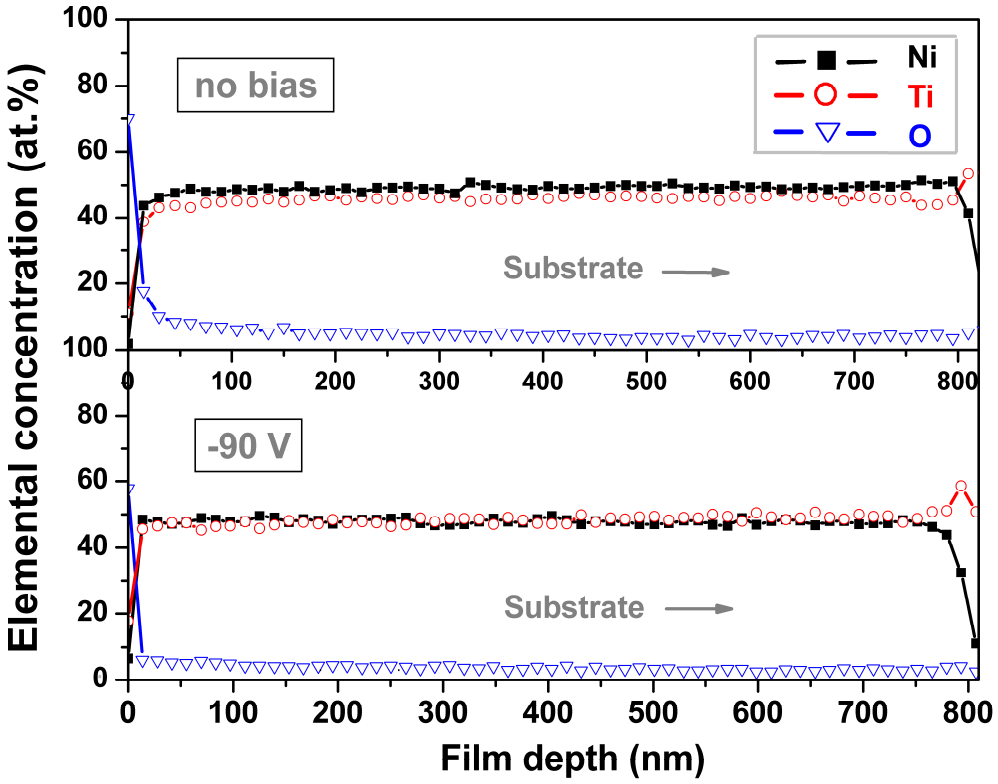
no bias
Ni
Ti
O
Substrate
-90 V
Substrate
Elemental concentration (at.%)
Film depth (nm)
0
20
40
60
80
100
0
100
200
300
400
500
600
700
800

FIGURE 5

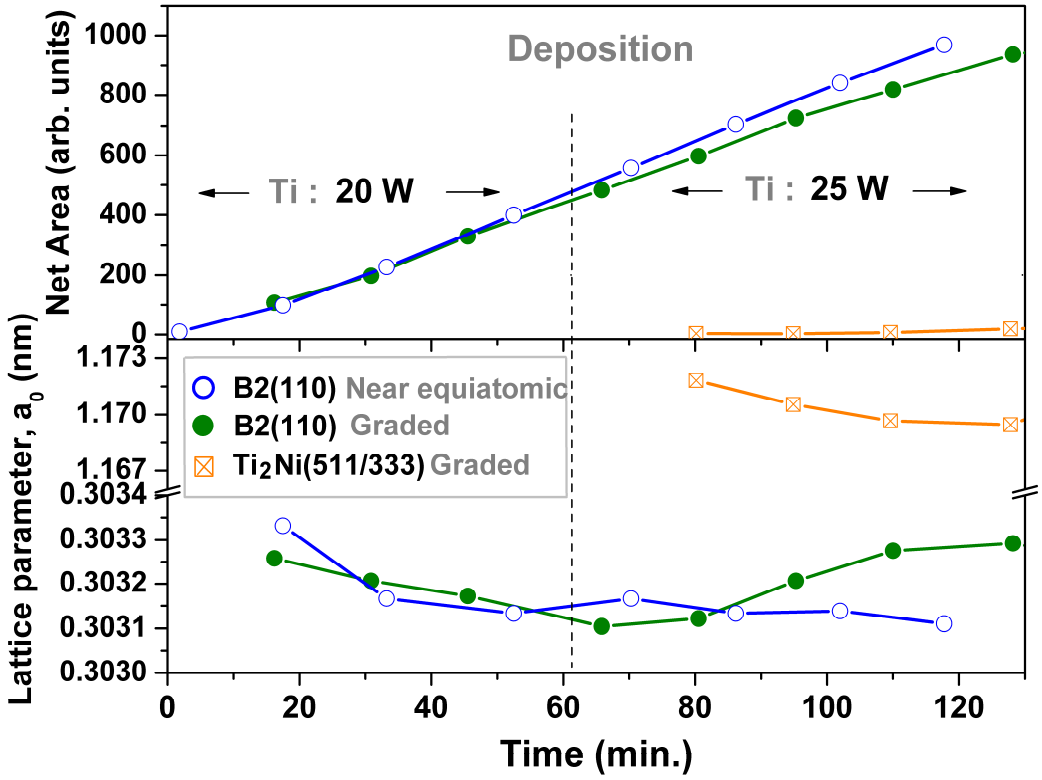
Deposition
Ti : 20 W
Ti : 25 W
Net Area (arb. units)
1000
800
600
400
200
0
Lattice parameter, a_0 (nm)
1.173
1.170
1.167
0.3034
0.3033
0.3032
0.3031
0.3030
B2(110) Near equiatomic
B2(110) Graded
Ti_2Ni(511/333) Graded
0
20
40
60
80
100
120
Time (min.)

FIGURE 6

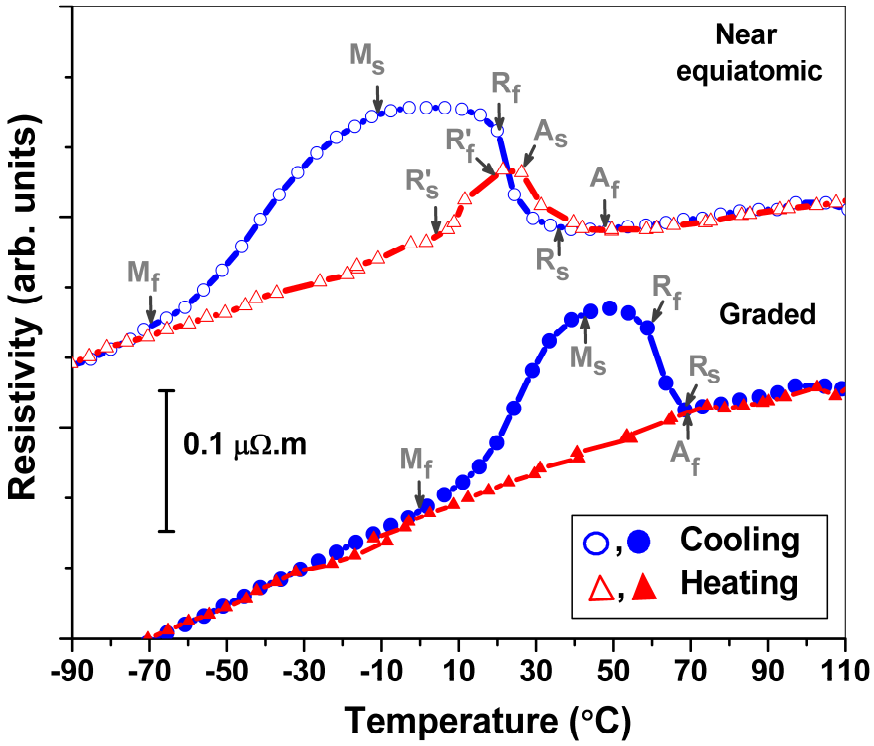
Near
equiatomic
Graded
Resistivity (arb. units)
Temperature (°C)
0.1 μΩ.m
Cooling
Heating
Ms
Rf
R'f
As
Af
R's
Rs
Mf
-90
-70
-50
-30
-10
10
30
50
70
90
110

FIGURE 7